Structure of the Bis Divalent Cation Complex with Phosphonoacetohydroxamate at the Active Site of Enolase†

Russell R. Poyner and George H. Reed*

Institute for Enzyme Research, Graduate School, and Department of Biochemistry, College of Agricultural and Life Sciences, University of Wisconsin—Madison, Madison, Wisconsin 53705

Received March 16, 1992; Revised Manuscript Received May 6, 1992

ABSTRACT: Phosphonoacetohydroxamate (PhAH) is a tight-binding (K_i = 15 pM) inhibitor of enolase that is believed to mimic the *aci*-carboxylate form of the intermediate carbanion in the reaction [Anderson, V. E., Weiss, P. M., & Cleland, W. W. (1984) *Biochemistry 23*, 2779]. Electron paramagnetic resonance (EPR) spectroscopy of Mn^{2+} has been used to map sites of interaction of PhAH with the two divalent cations at the active site of enolase from bakers' yeast. EPR spectra of enolase–PhAH complexes containing two Mn^{2+} bound at the active site contain multiple fine structure transitions each with a 45-G ^{55}Mn hyperfine spacing that is a characteristic of spin exchange coupled pairs of Mn^{2+}. Magnetically dilute complexes were obtained by preparation of specific Mg^{2+}/Mn^{2+} hybrid complexes by manipulating the order of addition of the divalent metal species. Thus, Mn^{2+} was placed in the higher affinity site by addition of 1 equiv of Mn^{2+} to a solution of enolase and PhAH, followed by addition of 1 equiv of Mg^{2+}. Reversing the order of addition of Mg^{2+} and Mn^{2+} placed Mn^{2+} in the lower affinity site. Regiospecifically ^{17}O-labeled forms of PhAH were prepared, and the binding of the functional groups on PhAH to Mn^{2+} at the two metal ion sites was determined from the presence or absence of ^{17}O superhyperfine coupling in the EPR signals. The hydroxamate oxygen is a ligand of Mn^{2+} at the higher affinity site, a phosphonate oxygen is a ligand of Mn^{2+} at the lower affinity site, and the carbonyl oxygen is a μ–O bridge of the two metal ions. The binuclear chelate structure of the bound inhibitor suggests electrophilic roles for both divalent cations in stabilization of the *aci*-carboxylate form of the intermediate carbanion as well as an electrophilic role of the high-affinity metal ion in augmenting the leaving group ability of the 3-OH of 2-phospho-D-glycerate.

Enolase catalyzes the reversible dehydration of 2-phospho-D-glycerate (2-PGA)[1] to produce P-enolpyruvate. The reaction appears to include formation of a carbanion at C-2, and catalysis occurs through specific stabilization of this carbanion intermediate (Dinovo & Boyer, 1971; Stubbe & Abeles, 1980; Anderson & Cleland, 1990). Two equivalents of divalent cation are required per active site for catalysis (Faller et al., 1977). The enzyme binds 1 equiv of divalent metal ion per subunit (site I) with high affinity in the absence of substrates, and binding of a second equivalent of divalent cation (site II), required for catalysis, is synergized by the presence of substrate or an analogue thereof (Faller et al., 1977; Anderson et al., 1984). Additional equivalents of metal ions bind with weaker affinities, and occupation of these sites is inhibitory (Faller et al., 1977). The potential for electrophilic catalysis by divalent cations is conspicuous in this mechanism (Brewer, 1981). One or both of the metal ions could participate in stabilizing the carbanion intermediate, and one of the cations may assist the leaving group ability of the 3-OH and activate a water molecule (through ionization to OH^-) in the reverse direction (Nowak et al., 1973). X-ray crystallographic studies have revealed the location of the active site and of the higher-affinity binding site for one of the metal ions (Lebioda et al., 1989; Lebioda & Stec, 1989). A subsequent structure obtained from crystals of enolase with one metal ion and substrate in the active site suggests that the 3-OH group of 2-PGA binds directly to this metal ion (Lebioda & Stec, 1991).

Anderson et al. (1984) prepared a series of inhibitors that mimicked the structure of the proposed carbanion intermediates of the enolase reaction. The design of these inhibitors was based on experience with other enzymic elimination reactions in which putative carbanion intermediates are α to a carboxylate group such as in the reactions catalyzed by aspartase, fumarase, and aconitase (Porter & Bright, 1980; Schloss et al., 1980). The intermediate carbanions in these reaction are thought to be stabilized by formation of an *aci*-carboxylate (**1**) wherein the negative charge is delocalized onto the carboxylate oxygens. Surprisingly, the most potent

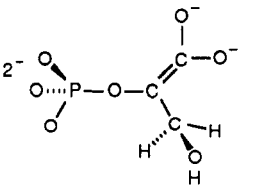

1

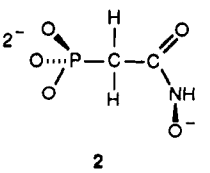

2

inhibitor of enolase, PhAH (**2**) (K_i = 15 pM for the ionized form shown, pK_a = 10.2), lacks a carboxylate functionality (or nitro analogue thereof) but does possess an sp^2-hybridized carbon at the position corresponding to C-2 of the substrate (Anderson et al., 1984).

The crystallographic data obtained thus far have been from crystals grown and manipulated at acidic pH's in concentrated ammonium sulfate where there is evidently resistance to

† This work was supported by NIH Grant GM35752 (G.H.R.). R.R.P. was supported during part of this work by a NRSA from NIH Training Grant GM 07215.

[1] Abbreviations: 2-PGA, 2-phospho-D-glycerate; P-enolpyruvate, phosphoenolpyruvate; EPR, electron paramagnetic resonance; NMR, nuclear magnetic resonance; PhAH, phosphonoacetohydroxamate; PMSF, phenylmethanesulfonylfluoride; Hepes, 4-(2-hydroxyethyl)-1-piperazineethanesulfonic acid; *D*, the axial zero-field splitting parameter; *E*, the rhombic zero-field splitting parameter.

0006-2960/92/0431-7166$03.00/0

binding of the second equivalent of Mg^{2+} (Lebioda & Stec, 1991). The position of this second cation may be crucial to understanding the exact position of the substrate and the roles of the cations in the mechanism. For example, earlier EPR studies of Mn^{II}–enolase at 77 K (Chien & Westhead, 1971) had revealed a prominent Mn^{2+}–Mn^{2+} spin exchange coupling that is normally mediated by a bridging ligand. Recently, Lee and Nowak (1992) have suggested that the second metal ion does not bind at the active site but at a site >12 Å from the first metal ion. Curiosity regarding the location of the second metal ion on enolase, as well as interest in the structural basis for the 14.8 kcal mol^{-1} binding affinity of PhAH, stimulated interest in spectroscopic studies of bis metal complexes of enolase with this inhibitor. The present paper reports the results of Mn^{2+} EPR studies with specifically ^{17}O-labeled forms of PhAH.

EXPERIMENTAL PROCEDURES

Enolase. Enolase was isolated from bakers' yeast by slight modifications of procedures described previously (Westhead, 1966; Westhead & McLain, 1964). PMSF (0.45 g of PMSF/lb of yeast) was added at the start of the toluene autolysis step. An additional 0.23 g of PMSF/lb of yeast was added after excess toluene was decanted. Tris/EDTA, pH 8.2, was added during the water extraction step to a final concentration of 1 mM. The final treatment with phosphocellulose was replaced by DEAE-Sephacel chromatography at room temperature. When starting with 5 lb of yeast, a 2.6 × 35 cm column was sufficient. The column was equilibrated with a buffer (buffer A) consisting of 1 mM Tris/acetic acid, pH 8.0, with 1 mM $Mg(OAc)_2$. The clear filtrate obtained after the batch treatment with DEAE-cellulose was adjusted to pH 8.5 with 2N NH_3(aq) and applied to the column. The column was then washed with buffer A until the absorbance of the eluate at 280 nm returned to baseline. The column was then eluted with a 2-L linear gradient from buffer A to 100 mM Tris/acetic acid, pH 8.0, with 1 mM $Mg(OAc)_2$. Three separate peaks containing active enolase were typically obtained, and only fractions with specific activity above 155 IU mg^{-1} from the first peak were used. The enzyme was stored at 4 °C in polyethylene tubes at ~40 mg/mL, in buffer A to which 0.1 mM EDTA and 0.02% NaN_3 was added.

Enolase Assay. Enolase was assayed spectrophotometrically as described by Westhead (1966). Enzyme concentrations were calculated from the absorbance at 280 nm assuming $\epsilon = 0.89$ cm^{-1} mg^{-1} mL^{-1} and a subunit molecular weight of 46 500 (Chin et al., 1981a,b; Holland et al., 1980).

Apoenolase. Stock solutions of enzyme for EPR measurements were prepared by equilibration of purified enolase into a buffer of 50 mM Hepes/HCl, pH 7.5, and 0.1 M KCl by gel filtration over a column of Sephadex G50. Solutions of protein were then passed through a 1.5 × 40 cm column of Chelex 100 equilibrated in the same buffer. Finally, the protein was concentrated by vacuum dialysis using a collodion bag apparatus.

Unlabeled PhAH. Unlabeled PhAH was synthesized as described by Anderson et al. (1984) and purified by anion exchange on a 2.6 × 30 cm column of Dowex AG-MP-1, 200–400 mesh in 10 mM imidazole/HCl, pH 6.8; eluted with a 1.5-L gradient from 50 to 100 mM LiCl. PhAH was located by total phosphorus analysis and by ferric chloride assay using $\epsilon_{505} = 275$ M^{-1} cm^{-1} (Anderson et al., 1984). Fractions that contained PhAH (as judged by ferric chloride assay) frequently contained other compounds with phosphorus. When this overlap occurred, the fractions containing PhAH were pooled and rechromatographed until PhAH was obtained as a separate fraction. The purified PhAH was lyophilized and washed with 25% methanol in acetone to remove LiCl.

Phosphonate ^{17}O-Labeled PhAH. The phosphonate oxygens of PhAH were labeled by displacing the chlorides of ethylacetylphosphonyl dichloride with $H_2{}^{17}O$ and by reacting the resulting ethylphosphonoacetate with hydroxylamine as in the synthesis of the unlabeled compound. Ethylacetylphosphonyl dichloride was synthesized from triethylphosphonoacetate as described by Bhongle et al. (1987). The orange oil produced was confirmed to be ethylacetylphosphonyl dichloride by ^{13}C NMR and was used without purification. Duplicate samples of the dichloride were reacted with normal water or 51.1 atom% ^{17}O water (Monsanto) in dry tetrahydrofuran. After 2 h the reactions were diluted with normal water, and the labeled ethylphosphonoacetate was converted to PhAH, which was then purified by anion-exchange chromatography as described above.

Hydroxamate ^{17}O-Labeled PhAH. ^{17}O was incorporated into the hydroxamate oxygen of PhAH by first preparing labeled hydroxylamine from the reaction of $Na[^{17}O]NO_2$ (34 atom % ^{17}O) and $BH_3{\cdot}S(CH_3)_2$ (Rajendran & Van Etten, 1986). The hydroxylamine in the product mixture did not react with ethylphosphonoacetate, apparently due to an interfering coproduct. However, the synthetic hydroxylamine did react cleanly with triesters of phosphonoacetic acid.

The unpurified, labeled hydroxylamine produced from 300 μmol of $Na[^{17}O]NO_2$ was converted to *p,p*-dimethyl PhAH by reaction with 250 μL of trimethylphosphonoacetate at pH 13 for 1 h. The product was then demethylated by two cycles of acidification with Dowex 50W H^+ and treatment with NaI in dry acetone (Zervas & Dilaris, 1955; Kluger et al., 1990). PhAH and monomethyl PhAH were separated by anion-exchange chromatography, and the fraction containing monomethyl PhAH was acidified with Dowex 50W H^+ and retreated with NaI. Fractions of labeled PhAH were combined and purified by anion-exchange chromatography as described above. A sample of unlabeled PhAH was prepared by the same procedure.

Carbonyl ^{17}O-Labeled PhAH. PhAH labeled in the carbonyl oxygen was prepared by exchanging the carboxylate oxygens of phosphonoacetic acid with $H_2{}^{17}O$ and then converting the labeled acid to PhAH as described for the unlabeled compound. Phosphonoacetic acid (70 mg), 51.1 atom% $H_2{}^{17}O$ (50 μL), and dry Dowex 50W X8 H^+ (50 mg) were combined in a dry Wheaton vial. The vial was sealed and heated at 50 °C for 2 days. Water was then removed by lyophilization, and 400 μL of anhydrous ethanol was added. The vial was resealed and heated at 50 °C overnight. The resulting labeled ethylphosphonoacetate was converted to PhAH and purified as described above for the unlabeled compound.

K^+ Salts of PhAH. PhAH was converted from the Li^+ salt to the K^+ salt by passage through a small column of Dowex 50W X8 H^+ to generate the free acid and then neutralized with KOH.

Phosphorus Assays. Total phosphorus assays were performed by ashing an aliquot of the sample with $Mg(NO_3)_2$ (Ames, 1966). Phosphate was then measured spectrophotometrically using the ammonium molybdate, malachite green method (Tashima & Yoshimura, 1975).

Sample Preparation. Stock solutions of ^{17}O-labeled PhAH were matched in concentration to the corresponding unlabeled solutions to ±5% using the ferric chloride assay. In cases where the EPR spectrum changed with time, the

experiment was timed, so that the time interval between the addition of the final component of the sample and the recording of the spectrum was the same for matched samples to within 15 s. Amplitudes of EPR signals from duplicate samples prepared by these procedures matched within ±2%. Samples in ^{17}O-enriched water were prepared by two methods: (1) lyophilization and hydration in ^{17}O-enriched water and (2) dilution of a concentrated sample with an equal volume of ^{17}O-enriched water.

EPR Measurements. Q-band (35 GHz) EPR spectra were recorded with a Varian E109Q spectrometer. Sample temperature was maintained at 2 ± 1 °C with a Varian flow dewar and temperature controller. Low-temperature spectra were recorded at X-band (9.2 GHz) with a Varian E Line spectrometer equipped with a E-102 microwave bridge and an Oxford Instruments ESR 900 continuous-flow helium cryostat. Both spectrometers were interfaced with AT microcomputers for data acquisition. Spectra were simulated as described previously (Reed & Markham, 1984).

EPR Methodology. Oxygen ligands for Mn^{2+} were identified from ^{17}O-labeled Mn^{2+} superhyperfine coupling which induces inhomogeneous broadening in the EPR signals for Mn^{2+} (Reed & Leyh, 1980). The number of water ligands for Mn^{2+} was determined from comparison of EPR signals for Mn^{2+} in normal water and in ^{17}O-enriched water using the difference spectrum method described earlier (Reed & Leyh, 1980; Lodato & Reed, 1987; Smithers et al., 1990). To improve the contrast in the difference method for obtaining hydration numbers, the EPR signals were resolution enhanced using Fourier deconvolution methods (Kauppinen et al., 1981; Latwesen et al., 1992). The spectral data were uploaded to a VAX workstation for resolution enhancement and analysis.

For an isolated Mn^{2+} ($S = {}^5/_2$) bound in an enzymic complex, the dominant EPR signals arise from the $m_s = {}^1/_2 \leftrightarrow m_s = -{}^1/_2$ electron spin (fine structure) transition. This transition is split into a sextet by hyperfine coupling to the nuclear spin of ^{55}Mn ($I = 5/2$). In complexes with octahedral geometry, the ^{55}Mn hyperfine coupling constant, $|A|$, is ~90 G (0.0084 cm^{-1}). Signals in the $m_s = {}^1/_2 \leftrightarrow m_s = -{}^1/_2$ transition can exhibit additional structure due to anisotropy arising from second-order effects of the zero-field splitting interaction (Reed & Markham, 1984).

The EPR properties of spin-exchange coupled pairs of Mn^{2+} are more complicated than those of a magnetically isolated ion (Abragam & Bleaney, 1970). The number of fine structure transitions depends upon the magnitude and sign of the Mn^{2+}–Mn^{2+} spin-exchange coupling constant, J, and the temperature (Owen & Harris, 1972). The exchange interaction couples the two $S = {}^5/_2$ centers into a manifold of new states with total spin, $\boldsymbol{S}$, of 0, 1, 2, 3, 4, or 5. When J is negative (ferromagnetic coupling), the ground state is $\boldsymbol{S} = 5$, whereas when J is positive (antiferromagnetic coupling) the ground state is diamagnetic, $\boldsymbol{S} = 0$. In each case, excited states are spaced according to the Lande interval, but appreciable deviations in this spacing have been documented (Harris, 1972). Even in cases of antiferromagnetic coupling, if $J \leq$ 1–3 cm^{-1}, excited paramagnetic states ($\boldsymbol{S} > 0$) have significant populations—even at 4 K. The isotropic part of the exchange interaction can result from direct overlap of metal *d* orbitals or it may be mediated through orbitals of a bridging ligand (superexchange). The through-space dipole–dipole coupling of the ions contributes to the anisotropic zero-field splitting interaction. Mn^{2+}–Mn^{2+} spin coupling is readily diagnosed in an EPR spectrum because of the appearance of multiline patterns in which the ^{55}Mn hyperfine spacing is half (~45 G) of its value for an isolated ion (Abragam & Bleaney, 1970). When $J \gg |A|$, the spectrum consists of fine structure transitions ($\Delta m_s = \pm 1$) within $\boldsymbol{S} > 0$ states in which each transition consists of 11 lines at intervals of $A/2$ (~45 G) with relative intensities of 1:2:3:4:5:6:5:4:3:2:1. When $J \approx |A|$, there can be more lines, and the spacing can deviate from $A/2$ (Wilkins & Culvahouse, 1976; Markham, 1981).

RESULTS

Enolase–Mn^{2+}–PhAH Complexes. When Mn^{2+} is titrated into a solution of enolase and PhAH, the appearance of the EPR spectrum changes with the ratio of Mn^{2+} to enolase, and there is a time dependence of the spectra at higher ratios of Mn^{2+} to enolase. Spectra from three points in such a titration are shown in Figure 1A. At a ratio of Mn^{2+} to enolase active sites of 0.1 there is no time dependence, and the signals in the spectrum are narrow. All of the features in this spectrum can be simulated with a single set of Hamiltonian parameters (D = 270 G, $E/D = {}^1/_3$) corresponding to a single species of bound Mn^{2+}. At ratios of Mn^{2+} to enolase of 0.5:2.0 the spectrum obtained initially contains a single set of six sharp signals and an underlying spectrum that consists of >36 signals with a spacing of ~45 G. This multiline pattern is diagnostic of Mn^{2+}–Mn^{2+} electron spin-exchange coupling (Reed & Markham, 1984). The presence of signals for the exchange-coupled pairs of Mn^{2+} at ratios of Mn^{2+}:enolase active sites of <1 indicates that PhAH synergizes binding of the second metal ion. The intensity of the exchange-coupled pattern increases, and there are subtle changes in the central features of the spectrum when the sample is left at room temperature overnight. The time dependence of these spectra parallels that observed for Mg^{2+}/Mn^{2+} hybrid complexes and may be related to the slow binding inhibition behavior of PhAH (Anderson et al., 1984).

X-band EPR spectra of the enolase–$(Mn^{II})_2$–PhAH complex at 4–6 K are more complex than Q-band spectra taken at 275 K. The spectra (see Figure 1B) exhibit multiple fine-structure transitions. The number of fine-structure transitions in the spectrum indicates that spin states with $\boldsymbol{S} > 1$ are populated at these low temperatures. This result indicates that $|J| \approx$ 1–3 cm^{-1}.

Enolase–PhAH–Mg^{2+}/Mn^{2+} Hybrid Complexes. In order to facilitate ligand mapping experiments of the individual metal sites in bis metal complexes, it is necessary to break the spin-exchange coupling by inserting a diamagnetic metal ion as a partner for the spectroscopic probe, Mn^{2+}, in hybrid bis metal species as has been done with pyruvate kinase (Lodato & Reed, 1987; Buchbinder & Reed, 1990). While it might be possible to exploit the intrinsic selectivities of the two sites for different species of divalent cation, the tight binding, slow dissociation properties of PhAH permit experimental manipulation of the positions of Mn^{2+} and its diamagnetic partner simply by varying the order of addition of Mn^{2+} and the companion divalent cation to samples of enolase and PhAH. Thus, the spectrum of Mn^{2+} bound at site I is obtained by addition of first Mn^{2+} then Mg^{2+} to the PhAH/enolase mixture (Figure 2). Reversing the order of addition of Mn^{2+} and Mg^{2+} permits observation of the spectrum of Mn^{2+} bound at site II (Figure 3). The environments of Mn^{2+} in sites I and II differ and give rise to different EPR spectra.

Spectra of the Mn^{2+}/Mg^{2+} hybrid complexes show two types of time dependence. First, there are changes in the spectra with time when Mn^{2+} is at either site. These spectral changes occur with half lives of the order of 5–10 min at 25 °C, and this time scale is similar to that reported (Anderson

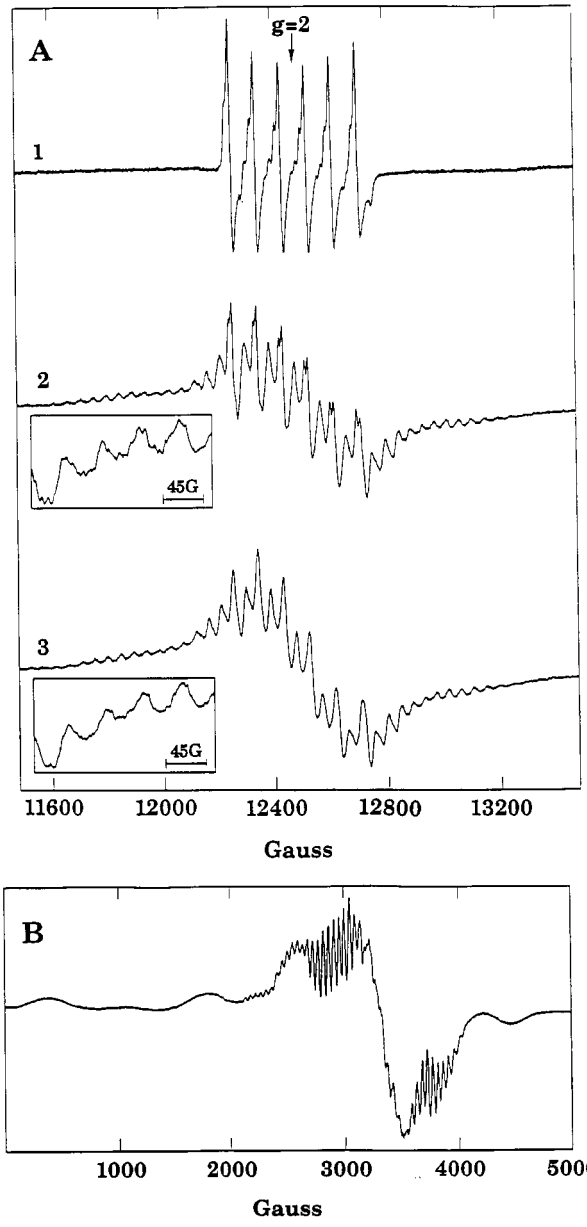

FIGURE 1: (A) Q-band (35 GHz) EPR spectra of enolase–Mn^{II}–PhAH complexes at 273 K. (1) Enolase–Mn^{II}–PhAH complex; Mn^{2+}:E ratio = 0.1 (6.6 mM enolase active sites, 640 μM $MnCl_2$, 17 mM PhAH, 50 mM Hepes, 0.1 M KCl, pH 7.5). (2) Enolase–Mn^{II}–PhAH complex; Mn^{2+}:E ratio = 1.0 after equilibration at 20 °C for 15 h (5.3 mM enolase active sites, 5.3 mM $MnCl_2$, 14 mM PhAH, 50 mM Hepes, 0.1 M KCl, pH 7.5). (3) Enolase–Mn^{II}–PhAH complex; Mn^{2+}:E ratio = 2.0 after equilibration at 20 °C for 15 h (5.3 mM enolase active sites, 10 mM $MnCl_2$, 14 mM PhAH, 50 mM Hepes, 0.1 M KCl, pH 7.5). (Insets) Expansion of spectra from 12850 to 13050 G, showing part of the spin-exchange pattern with 45 G ^{55}Mn hyperfine splitting. (B) X-band (9 GHz) spectrum of enolase bis Mn^{2+}–PhAH complex at 6 K (350 μM enolase active sites, 700 μM $MnCl_2$, 1 mM PhAH, 50 mM Hepes, 0.1 M KCl, pH 7.5).

et al., 1984) for the slow binding inhibition of Mg^{2+}-activated enolase by PhAH. The second type of time dependence is observed only when Mn^{2+} is added to the sample last. In this case Mn^{2+} starts out at site II but slowly exchanges with the Mg^{2+} at site I until virtually all of the Mn^{2+} has migrated to site I—the thermodynamically governed distribution of Mn^{2+} and Mg^{2+} between the two sites. The time scale for this site–site exchange varies from hours at 25 °C to several days at 0 °C—a time scale consistent with the slow dissociation of PhAH from the enzyme (Anderson et al., 1984). The amplitudes of EPR signals of the two different Mn^{2+}/Mg^{2+}

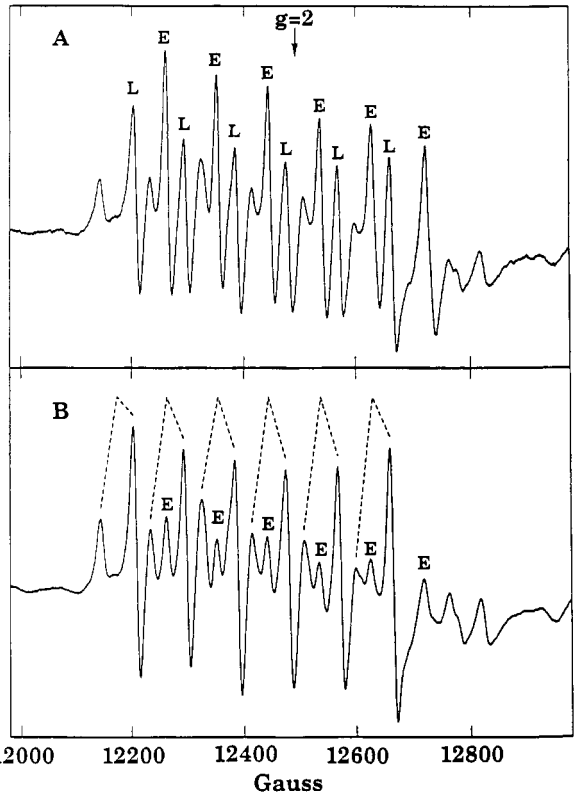

FIGURE 2: EPR spectra of enolase–Mn^{II}–PhAH–Mg^{II} complex; Mn^{2+} at site I. (A) Enolase–Mn^{II}–PhAH–Mg^{II} 3 min after addition of Mg^{2+} (4.9 mM enolase active sites, 3.3 mM $MnCl_2$, 19 mM PhAH, 11 mM $MgCl_2$, 50 mM Hepes, 0.1 M KCl, pH 7.5). E indicates signals associated with the early-time, sharp species, L indicates the central feature of the anisotropic signal that dominates at equilibrium. (B) Enolase–Mn^{II}–PhAH–Mg^{II} at equilibrium (4.9 mM enolase active sites, 3.3 mM $MnCl_2$, 19 mM PhAH, 11 mM $MgCl_2$, 50 mM Hepes, 0.1 M KCl, pH 7.5). The sets of dashed lines connect the upfield portion of the anisotropic signal with the central feature of the ^{55}Mn hyperfine transition. This pattern is due to a single species of Mn^{2+} as it can be simulated with a single set of hamiltonaian parameters (D = 600 G, E = 144 G). E indicates signals due to the residual, early-time species.

hybrid complexes are, however, reproducible at a given time following mixing to permit quantitation of ^{17}O-induced inhomogeneous broadening in the signals.

Experiments with Hydroxamate, Phosphonate, and Carbonyl-Labeled PhAH. Using the order of addition of Mn^{2+} and Mg^{2+} to direct Mn^{2+} to either site I or site II, the possibility for direct binding of the hydroxamate, phosphonate, and carbonyl oxygens in PhAH to each of the metal centers was explored with the respective ^{17}O-labeled froms of the inhibitor. Results of EPR measurements with [H^{17}O-N]PhAH and with [^{17}O-P]PhAH are summarized in Figure 4. These data show that the hydroxamate oxygen binds to Mn^{2+} at site I and that a phosphonate oxygen binds to Mn^{2+} at site II. The aforementioned, short half-life changes in the spectra are not connected with binding of the hydroxamate oxygen to Mn^{2+} at site I or to binding of the phosphonate ligand to Mn^{2+} at site II, because the pattern of ^{17}O-induced inhomogeneous broadening is evident in signals obtained both early and late during this process.

Results of EPR measurements of samples with ^{17}O in the carbonyl oxygen of PhAH are summarized in Figure 5. These data show that the carbonyl oxygen of PhAH coordinates to Mn^{2+} when the Mn^{2+} is either at site I or at site II. Binding of the carbonyl oxygen from PhAH to metals at both sites demonstrates that this oxygen functions as a μ–O bridge for the two divalent cations. The presence of this μ–O bridge

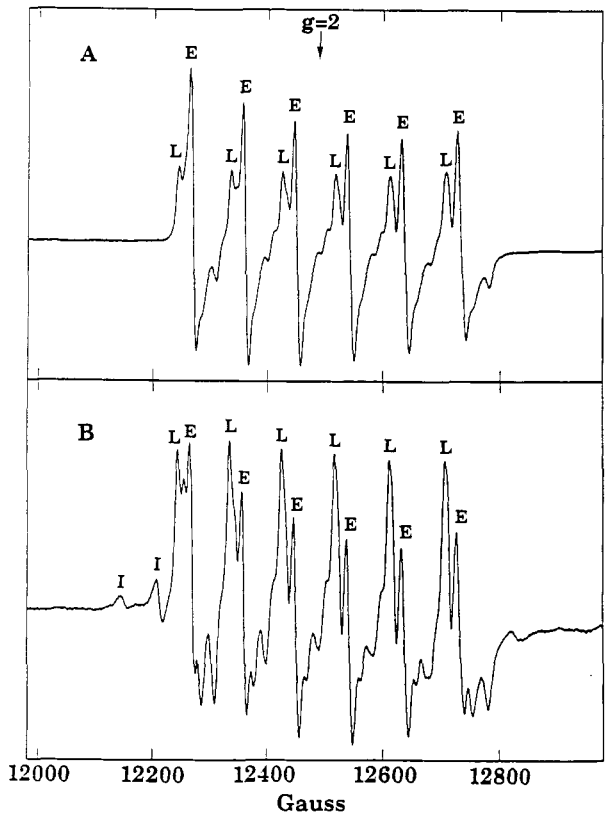

FIGURE 3: EPR spectra of enolase–Mg^{II}–PhAH–Mn^{II} complex, Mn^{2+} at site II. (A) Enolase–Mg^{II}–PhAH–Mn^{II} complex 2 min 40 s after addition of Mn^{2+} (4.8 mM enolase active sites, 6.5 mM $MgCl_2$, 14 mM PhAH, 2.0 mM $MnCl_2$, 50 mM Hepes, 0.1 M KCl, pH 7.5). E indicates signals associated with the early-time species; L indicates signals associated with the late-time species. (B) Enolase–Mg^{II}–PhAH–Mn^{II} complex after incubation for 23 h at 0 °C (4.8 mM enolase active sites, 6.5 mM $MgCl_2$, 14 mM PhAH, 2.0 mM $MnCl_2$, 50 mM Hepes, 0.1 M KCl, pH 7.5). E indicates signals due to residual, early-time species. L indicates signals associated with the late-time species. I indicates signals due to Mn^{2+} that has migrated to site I.

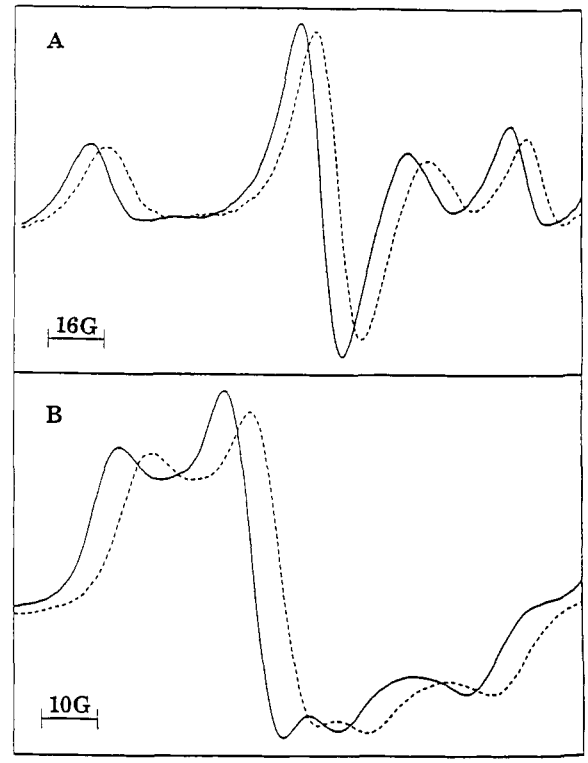

FIGURE 4: EPR spectra of complexes with [^{17}O-N]PhAH (34 atom % ^{17}O), and [$^{17}O_3$-P]PhAH (30 atom % ^{17}O). (A) First ^{55}Mn hyperfine transition of the spectrum of the enolase–Mn^{II}–PhAH–Mg^{II} equilibrium complex with [^{17}O-N]PhAH (4.8 mM enolase active sites, 3.2 mM $MnCl_2$, 8 mM PhAH, 9.2 mM $MgCl_2$, 50 mM Hepes, 0.1 M KCl, pH 7.5). (B) First ^{55}Mn hyperfine transition of the spectrum of the enolase–Mg^{II}–PhAH–Mn^{II} complex with [$^{17}O_3$-P]-PhAH (3.4 mM enolase active sites, 4.9 mM $MgCl_2$, 18 mM PhAH, 1.8 mM $MnCl_2$, 50 mM Hepes, 0.1 M KCl, pH 7.5). In both panels A and B, solid curves correspond to spectra of unlabeled PhAH and dotted curves correspond to spectra of the respective ^{17}O-enriched PhAH. Spectra of labeled and unlabeled samples are offset by 5 G on the abscissa.

explains the strong Mn^{2+}–Mn^{2+} spin-coupling observed in the bis Mn^{2+} complexes with the inhibitor. The μ–O binuclear chelate coordination of enzyme-bound PhAH is shown schematically in Figure 6.

Binding of PhAH to Mn^{2+} at Site I. As shown in Figure 1A, at low ratios of Mn^{2+} to enolase it is possible to populate site I with Mn^{2+} without a second divalent cation at site II (enolase–Mn^{II}–PhAH). Under these conditions, it is likely that site II is occupied by a monovalent cation, because the appearance of the EPR spectrum changes when Li^+ is replaced by K^+ as the monovalent cation in the medium. This observation is consistent with the report of inhibition of enolase by Li^+ (Kornblatt & Musil, 1990). The hydroxamate and carbonyl oxygens of PhAH coordinate to Mn^{2+} at site I in this complex as evidenced by ^{17}O superhyperfine coupling in the EPR signals (data not shown).

$H_2{}^{17}O$ Studies. Hydration numbers of Mn^{2+} in the complexes with enolase and PhAH were determined by quantitative analysis of the ^{17}O-induced inhomogeneous broadening in EPR spectra of samples in solutions of ^{17}O-enriched water (see Experimental Procedures). At low ratios of Mn^{2+} to enolase, where the enolase–Mn^{II}–PhAH complex predominates, two water ligands are in the first coordination sphere of Mn^{2+}. The early time species found in the enolase–Mn^{II}–PhAH–Mg^{II} complex also has two water ligands. Mn^{2+} at site I, however, loses one of these water ligands upon conversion to the final enolase–Mn^{II}–PhAH–Mg^{II} complex (data not shown). This ligand exchange is therefore associated with the time dependent change in the EPR spectrum. Mn^{2+} at site II, however, does not change its hydration. Both the early and late forms of the enolase–Mg^{II}–PhAH–Mn^{II} complex have two water ligands. Data obtained from the complex with Mn^{2+} at site II are shown in Figure 7.

Enolase–Mn^{2+} Complexes. Chien and Westhead (1971) observed Mn^{2+}–Mn^{2+} spin-exchange coupling in EPR spectra for mixtures of Mn^{2+} and enolase at 77 K in the absence of substrates. This spin-exchange coupling is also evident in spectra obtained at much higher temperatures in the liquid phase for samples with ratios of Mn^{2+} to enolase active sites close to 1 (see Figure 8). The affinity of enolase for the second equivalent of Mn^{2+} is not as high in the absence of PhAH, and the central region of the spectrum contains some signals due to free Mn^{2+}. However, the presence of signals outside the envelope of the central transition that exhibit the signature 45 G spacing of spin-coupled pairs of Mn^{2+} (Figure 8B) shows that the enzyme binds two equivalents of Mn^{2+} per active site in the absence of substrate.

DISCUSSION

Results from EPR measurements on Mn^{2+}/Mg^{2+} hybrid complexes with ^{17}O-labeled forms of PhAH show that PhAH forms a binuclear chelate with the two metals and that the carbonyl oxygen of PhAH is a μ–O bridge (see Figure 6). Hydroxamates are well known for their high-affinity chela-

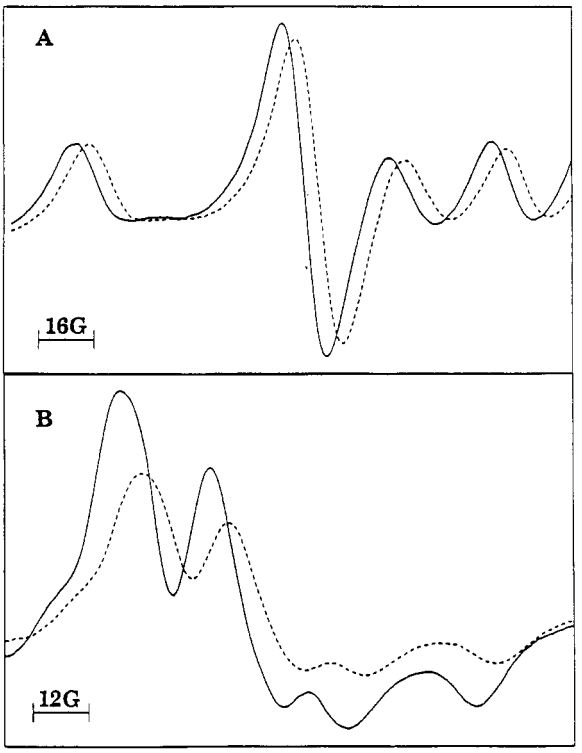

FIGURE 5: EPR spectra of complexes with [^{17}O-C]PhAH (37 atom % ^{17}O). (A) First ^{55}Mn hyperfine transition of the spectrum of the enolase–Mn^{II}–PhAH–Mg^{II} complex at equilibrium (4.9 mM enolase active sites, 3.3 mM $MnCl_2$, 19 mM PhAH, 11 mM $MgCl_2$, 50 mM Hepes, 0.1 M KCl, pH 7.5). (B) Sixth ^{55}Mn hyperfine transition of the spectrum of the enolase–Mg^{II}–PhAH–Mn^{II} complex after incubation for 23 h at 0 °C (4.8 mM enolase active sites, 6.5 mM $MgCl_2$, 14 mM PhAH, 2.0 mM $MnCl_2$, 50 mM Hepes, 0.1 M KCl, pH 7.5). In both panels A and B, solid curves correspond to spectra of unlabeled PhAH and dotted curves correspond to spectra of the [^{17}O-C]PhAH. Spectra of labeled and unlabeled samples are offset by 5 G on the abscissa.

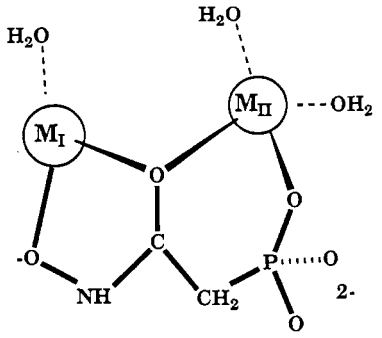

FIGURE 6: Schematic view of the μ–O binuclear coordination of PhAH. Water ligands are shown as determined for the equilibrium complex. In the preequilibrium complex, metal I binds a second water ligand. The positions of the water ligands in the coordination spheres of metals I and II relative to those of the ligands contributed by PhAH and by the protein are undetermined. Metal II appears to be hexacoordinate, so the protein contributes two ligands. Metal I might be either hexacoordinate or pentacoordinate (Lebioda & Stec, 1991) (see text), so there may be either three or two ligands from the protein in this complex.

tion of Fe^{3+}. Ions such as Mn^{2+} and Mg^{2+} are chelated by hydroxamates with lower affinities than Fe^{3+} (e.g., $pK_d = 4.0$ for the acetohydroxamate–Mn^{II} complex)(Smith & Martell, 1976). The parent compound, phosphonoacetate, is also an effective complexing agent [e.g., $pK_d = 5.6$ with Mg^{2+} (Farmer et al., 1981)]. The two chelate rings (five-membered with metal I and six-membered with metal II) that are formed at the active site must contribute substantially to the high thermodynamic stability of the inhibitor complex. The

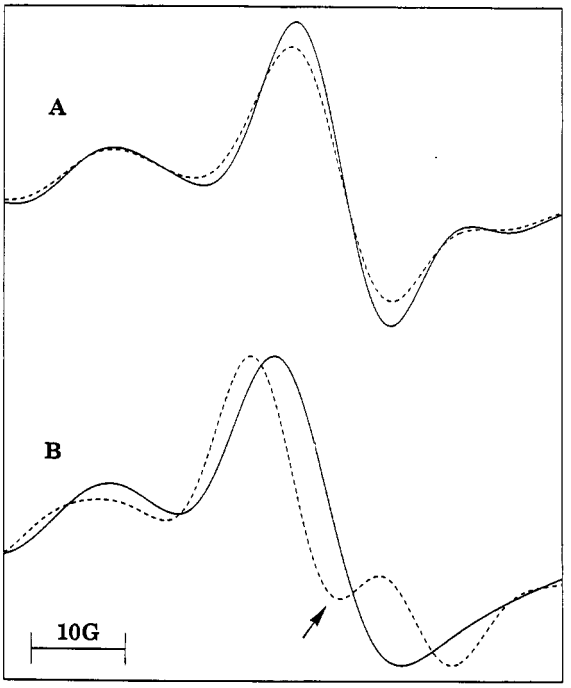

FIGURE 7: Hydration study of the enolase–Mg^{II}–PhAH–Mn^{II} early-time complex (Mn^{2+} at site II). (A) Experimental spectra (first ^{55}Mn hyperfine transition); solid curve, spectrum obtained in normal H_2O; dotted curve, spectrum obtained in 20 atom% $H_2{}^{17}O$. (B) Difference spectra; solid curve, spectrum obtained by subtraction assuming $2H_2O$ ligands (spectrum in 20 atom% $H_2{}^{17}O$ – 0.64 × spectrum in $H_2{}^{16}O$); dotted curve, spectrum obtained by subtraction assuming $1H_2O$ ligand (spectrum in 20 atom% $H_2{}^{17}O$ – 0.80 × spectrum in $H_2{}^{16}O$). The arrow indicates the location of the negative image of the spectrum of the sample in unenriched water in the difference spectrum corresponding to one water ligand. This negative image is absent in the difference spectrum corresponding to two water ligands. Samples contained 5.5 mM enolase active sites, 2.5 mM $MnCl_2$, 13 mM PhAH, 7.5 mM $MgCl_2$, 50 mM Hepes, and 0.1 M KCl, pH 7.5. Spectra in panel A were resolution enhanced (see Experimental Procedures) using a line width parameter of 10 G and truncation parameter in the time domain of 0.1 G^{-1}. All difference spectra were normalized to the same amplitude.

presence of two protein ligands for metal II, however, indicates that the inhibitor exploits an intrinsic site for this second metal ion. The energetically favorable, six-membered chelate ring at metal II in the complex with PhAH may account for the advantage in binding energy that PhAH holds over other inhibitors such as tartronate semialdehyde phosphate (Spring & Wold, 1971a,b) and 3-hydroxy-2-nitropropylphosphonate (Anderson et al., 1984). The chelate ring at metal II in analogous complexes with the latter inhibitors would contain seven atoms.

Anderson et al. (1984) postulated the existence of a slow unimolecular step to explain the slow binding inhibition of enolase by PhAH. The short half-life changes observed in the EPR spectra of enolase–PhAH–bis metal complexes are evidence of a structural change in these complexes that occurs upon addition of metal II. Furthermore, hydration studies show that the metal ion at site I loses a water ligand in the process. This structural change, observed spectroscopically, may be related to the slow unimolecular step in inhibition of enolase by PhAH. The drastically different concentrations of protein required in the kinetic and spectroscopic measurements, however, prevent a direct comparison of the respective kinetic constants.

The presence of the μ–O bridge from the carbonyl oxygen of PhAH in the bis Mn^{2+} complex with enolase is no doubt responsible for the prominent spin exchange interaction in the

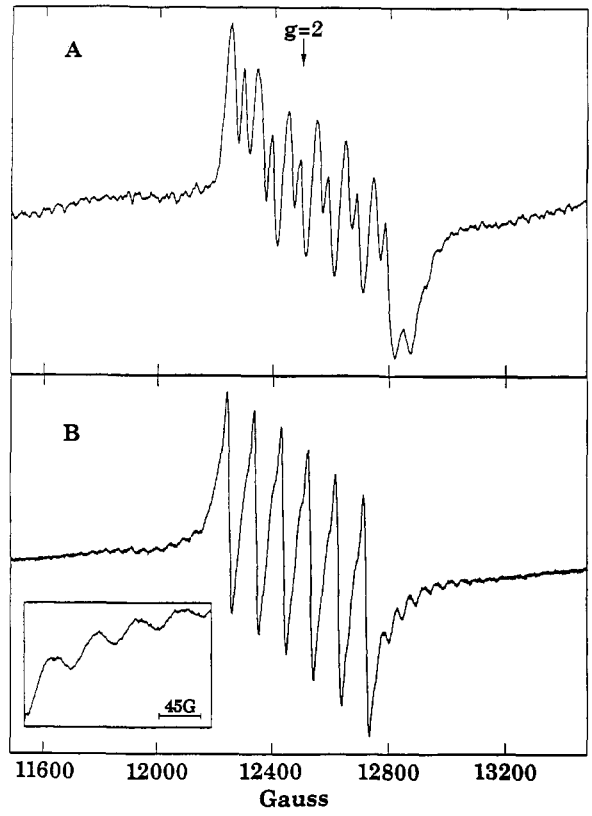

FIGURE 8: EPR spectra of enolase–Mn^{II} complexes. (A) Enolase–Mn^{II} complex Mn^{2+}:E ratio = 0.1 (7.3 mM enolase active sites, 710 μM $MnCl_2$, 50 mM Hepes, 0.1 M KCl, pH 7.5). (B) Enolase–Mn^{II} complex Mn^{2+}:E ratio = 1.0 (6.5 mM enolase active sites, 6.5 mM $MnCl_2$, 50 mM Hepes, 0.1 M KCl, pH 7.5). (Inset) Expansion of spectrum from 12850 to 13050 G, showing signals with 45 G spacing that is characteristic of spin-exchange coupling.

EPR signals for this complex. Molecular models indicate that the distance between the two Mn^{2+} ions is 3.2–3.8 Å in the complex. The identity of the bridging ligand in the complex without substrate or inhibitor present is not yet known. It is possible that a water molecule or OH^- serves as a μ–O bridge in the absence of substrate or inhibitor. However, the possibility that a functional group from the protein (e.g., a side-chain carboxylate) bridges the two cations cannot be eliminated. A μ,η^2 carboxylate ligand apparently mediates spin-exchange coupling in bis Mn^{2+} complexes of concanavalin A (Antanaitis et al., 1987).

EPR data reveal three ligands of Mn^{2+} at site I in the bis divalent cation complex with PhAH—the hydroxamate and carbonyl oxygens from PhAH and a water molecule. Crystallographic data have not yet been reported for this species, but a pentacoordinate metal I including three side-chain carboxylate ligands and two waters were indicated in the structure of the enolase–Mg^{II}–P-enolpyruvate complex (Lebioda & Stec, 1991). The anisotropic spectrum of Mn^{2+} at site I in the binuclear hybrid complex, enolase–Mn^{II}–PhAH–Mg^{II}, may arise from a pentacoordinate geometry. However, the substantial zero-field splitting anisotropy (D = 600 G, E/D = 0.24) observed in this complex could also arise from a distorted octahedral geometry (Reed & Markham, 1984). In the mononuclear enolase–Mn^{II}–PhAH species, the EPR spectrum reflects nearly cubic symmetry (D = 270 G, E/D = 1/3), and EPR data reveal two oxygens from PhAH and two water molecules as ligands. This coordination scheme leaves space for only two ligands from the protein to complete a hexacoordinate Mn^{2+} at site I. One water molecule leaves Mn^{2+} at site I upon binding of Mg^{2+} to site II. This scheme would lead to a pentacoordinate Mn^{2+} if only two of the side-chain carboxylates bind or to a hexacoordinate Mn^{2+} if all three side-chain carboxylates are ligands. EPR data identify four nonprotein ligands for metal II in the enolase–Mg^{II}–PhAH–Mn^{II} species. The protein must therefore contribute two ligands to this metal to complete octahedral coordination at site II.

Scheme I

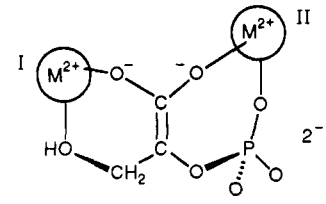

Analogous EPR data with regiospecifically labeled forms of the substrate and product are not yet available for enolase complexes. EPR spectra obtained from the equilibrium mixture of substrate and product with ratios of Mn^{2+} to enolase ≥1 do, however, exhibit spin-exchange coupling that requires an analogous close spacing of the two Mn^{2+} (R. R. Poyner & G. H. Reed, unpublished results). The exceptionally tight binding of PhAH to enolase implies that the structure of this complex should reveal key aspects of the natural strategy for stabilization of the carbanion intermediates (Anderson et al., 1984). This bis metal, μ–O chelate structure of enzyme-bound PhAH suggests an attractive structure for the analogous complex of the *aci*-carboxylate intermediate wherein the substrate carboxylate bridges the two metals ions (Scheme I). The chelate rings in this hypothetical structure are each one atom larger than the analogous rings in the complex of PhAH. Molecular models indicate that the six- and seven-membered rings in this structure are feasible. The larger chelate rings formed by the intermediate would promote freely reversible binding in the catalytic cycle.

The hypothetical structure of the intermediate complex (Scheme I) suggests electrophilic functions for both metal ions in catalysis. The bis metal chelate strategy would provide the electrophilic assistance required for promoting ionization of the carbon acid at C-2 (Gerlt et al., 1991), and this structure would be effective in stabilizing the *aci*-carboxylate intermediate. An electrophilic role for metal I in enhancing the leaving group ability of the 3-OH of 2-PGA [and in activating a water molecule for attack at C-3 of P-enolpyruvate (Nowak et al., 1973)] is also accommodated in this scheme.

PhAH is a member of a class of inhibitors of enolase that exhibit slow binding characteristics (Anderson et al., 1984). This class includes aminoenolpyruvate phosphate (Spring & Wold, 1971b), 3-hydroxy-2-nitropropylphosphonate, and phosphonopyruvate oxime (Anderson et al., 1984). All of these inhibitors resemble the putative *aci*-carboxylate intermediate in that they have an sp^2-hybridized carbon at the position analogous to C-2 and a potential ligand donor attached at a position analogous to C-3 of 2-PGA. Another tight binding inhibitor, tartronate semialdehyde phosphate, is closely related to the above class because it develops sp^2 hybridization at C-2 in an enolization step that follows initial binding (Lane & Hurst, 1974). The slow unimolecular step that occurs following binding of these, slow binding, intermediate analogues may reflect difficulties that are encountered in adjusting to the geometry of the intermediate state by an artificial route (Cleland, 1990). In the case of PhAH, this adjustment includes loss of a water molecule in the coordination sphere of metal I.

Gerlt et al. (1991) point out the kinetic advantage of concerted general acid–general base catalysis in achieving ionization of the carbon acids in enzyme catalyzed reactions. In enolase, a concerted Lewis acid–general base catalysis might involve entry of a substrate carboxylate oxygen into the coordination sphere of one of the divalent cations. Whether or not bis metal coordination of the carboxylate occurs in concert with the ionization at C-2 or in a discrete step, the coordination schemes of the metal ions in the substrate/product complexes may differ from those in the intermediate carbanion. Furthermore, the unusual pentacoordinate Mg^{2+} at site I (Lebioda & Stec, 1989) would be naturally poised to expand its coordination sphere to accept a carboxylate oxygen on the pathway to the intermediate. Hence, lack of Mg^{2+} coordination to the carboxylate of the substrate (product) in the structure derived from crystallography (Lebioda & Stec, 1991) may not be in conflict with the coordination scheme found here for PhAH (Figure 6) or with the hypothetical coordination scheme for the *aci*-carboxylate intermediate (Scheme I).

ACKNOWLEDGMENT

We are grateful to Dr. W. W. Cleland for suggesting spectroscopic studies of enolase inhibitor complexes. We thank Dr. Ronald Kluger for advice on demethylation of *p,p*-dimethyl PhAH. We also thank Bagels Forever of Madison, WI, for the generous gift of bakers' yeast.

REFERENCES

Abragam, A., & Bleaney, B. (1970) *Electron Paramagnetic Resonance of Transition Ions*, pp 491–535, Oxford University Press, London.
Ames, B. N. (1966) *Methods Enzymol. 8*, 115–118.
Anderson, V. E., & Cleland, W. W. (1990) *Biochemistry 29*, 10498–10503.
Anderson, V. E., Weiss, P. M., & Cleland, W. W. (1984) *Biochemistry 23*, 2779–2786.
Antanaitis, B. C., Brown, R. D., Chasteen, N. D., Freedman, J. H., Koenig, S. H., Lilienthal, H. R., Peisach, J., & Brewer, C. F. (1987) *Biochemistry 26*, 7932–7937.
Bhongle, N. N., Notter, R. H., & Turcotte, J. G. (1987) *Synth. Commun. 17*, 1071–1076.
Brewer, J. M. (1981) *CRC Crit. Rev. Biochem. 11*, 209–254.
Buchbinder, J. L., & Reed, G. H. (1990) *Biochemistry 29*, 1799–1806.
Chien, J. C. W., & Westhead, E. W. (1971) *Biochemistry 10*, 3198–3203.
Chin, C. C. Q., Brewer, J. M., Eckard, E., & Wold, F. (1981a) *J. Biol. Chem. 256*, 1370–1376.
Chin, C. C. Q., Brewer, J. M., & Wold, F. (1981b) *J. Biol. Chem. 256*, 1377–1384.
Cleland, W. W. (1990) *Biochemistry 29*, 3194–3197.
Dinovo, E. C., & Boyer, P. D. (1971) *J. Biol. Chem. 246*, 4586–4593.
Faller, L. D., Baroudy, B. M., Johnson, A. M., & Ewall, R. X. (1977) *Biochemistry 16*, 3864–3869.
Farmer, R. M., Heubel, P.-H. C., & Popov, A. I. (1981) *J. Solution Chem. 10*, 523–532.
Gerlt, J. A., Kozarich, J. W., Kenyon, G. L., & Gassman, P. G. (1991) *J. Am. Chem. Soc. 113*, 9667–9669.
Harris, E. A. (1972) *J. Phys. C: Solid State Phys. 5*, 338–352.
Holland, M. J., Holland, J. P., Thill, G. P., & Jackson, K. A. (1981) *J. Biol. Chem. 256*, 1385–1395.
Kauppinen, J. K., Moffatt, D. J., Mantsch, H. H., & Cameron, D. G. (1981) *Appl. Spectrosc. 35*, 271–276.
Kluger, R., Grant, A. S., Bearne, S. L., & Trachsel, M. R. (1990) *J. Org. Chem. 55*, 2864–2868.
Kornblatt, J. M., & Musil, R. (1990) *Arch. Biochem. Biophys. 277*, 301–305.
Lane, R. H., & Hurst, J. K. (1974) *Biochemistry 13*, 3292.
Latwesen, D. G., Poe, M., Leigh, J. S., & Reed, G. H. (1992) *Biochemistry 31*, 4946–4950.
Lebioda, L., & Stec, B. (1989) *J. Am. Chem. Soc. 111*, 8511–8513.
Lebioda, L., & Stec, B. (1991) *Biochemistry 30*, 2817–2822.
Lebioda, L., Stec, B., & Brewer, J. M. (1989) *J. Biol. Chem. 264*, 3685–3693.
Lee, M. E., & Nowak, T. (1992) *Biochemistry 31*, 2172–2180.
Lodato, D. T., & Reed, G. H. (1987) *Biochemistry 26*, 2243–2250.
Markham, G. D. (1981) *J. Biol. Chem. 256*, 1903–1909.
Nowak, T., Mildvan, A. S., & Kenyon, G. L. (1973) *Biochemistry 12*, 1690–1701.
Owen, J., & Harris, E. A. (1972) in *Electron Paramagnetic Resonance* (Geschwind, S., Ed.) pp 427–492, Plenum, New York.
Porter, D. J. T., & Bright, H. J. (1980) *J. Biol. Chem. 255*, 4772–4780.
Rajendran, G., & Van Etten, R. L. (1986) *Inorg. Chem. 25*, 876–878.
Reed, G. H., & Leyh, T. S. (1980) *Biochemistry 19*, 5472–5480.
Reed, G. H., & Markham, G. D. (1984) *Biol. Magn. Reson. 6*, 73–142.
Schloss, J. V., Porter, D. J. T., Bright, H. J., & Cleland, W. W. (1980) *Biochemistry 19*, 2358–2362.
Smith, R. M., & Martell, A. E. (1976) *Critical Stability Constants*; Vol. 3, p 301, Plenum, New York.
Smithers, G. W., Poe, M., Latwessen, D. G., & Reed, G. H. (1990) *Arch. Biochem. Biophys. 280*, 416–420.
Spring, T. G., & Wold, F. (1971a) *Biochemistry 10*, 4649–4654.
Spring, T. G., & Wold, F. (1971b) *Biochemistry 10*, 4655–4660.
Stubbe, J. A., & Abeles, R. H. (1980) *Biochemistry 19*, 5505–5512.
Tashima, Y., & Yoshimura, N. (1975) *J. Biochem. (Tokyo) 78*, 1161–1169.
Westhead, E. W. (1966) *Methods Enzymol. 9*, 670–676.
Westhead, E. W., & McLain, G. (1964) *J. Biol. Chem. 239*, 2464–2468.
Wilkins, R. W., & Culvahouse, J. W. (1976) *Phys. Rev. 14*, 1830–1841.
Zervas, L., & Dilaris, I. (1955) *J. Am. Chem. Soc. 77*, 5354.